Crystal Structure and Biochemical Characterization of Human Kallikrein 6 Reveals That a Trypsin-like Kallikrein Is Expressed in the Central Nervous System*

Matthew J. Bernett‡§, Sachiko I. Blaber‡, Isobel A. Scarisbrick¶, Pushparani Dhanarajan‖, Steven M. Thompson‖, and Michael Blaber‡§‡‡**

*From the ‡Institute of Molecular Biophysics, Departments of §Chemistry and Biochemistry and ‖Biological Science, and **School of Computational Science and Information Technology, Florida State University, Tallahassee, Florida 32306-4380 and the ¶Department of Neurology, Mayo Medical and Graduate School, Mayo Clinic Rochester, Rochester, Minnesota 55905*

The human kallikreins are a large multigene family of closely related serine-type proteases. In this regard, they are similar to the multigene kallikrein families characterized in mice and rats. There is a much more extensive body of knowledge regarding the function of mouse and rat kallikreins in comparison with the human kallikreins. Human kallikrein 6 has been proposed as the homologue to rat myelencephalon-specific protease, an arginine-specific degradative-type protease abundantly expressed in the central nervous system and implicated in demyelinating disease. We present the x-ray crystal structure of mature, active recombinant human kallikrein 6 at 1.75-Å resolution. This high resolution model provides the first three-dimensional view of one of the human kallikreins and one of only a few structures of serine proteases predominantly expressed in the central nervous system. Enzymatic data are presented that support the identification of human kallikrein 6 as the functional homologue of rat myelencephalon-specific protease and are corroborated by a molecular phylogenetic analysis. Furthermore, the x-ray data provide support for the characterization of human kallikrein 6 as a degradative protease with structural features more similar to trypsin than the regulatory kallikreins.

Recent studies demonstrate that humans have a large multigene family of at least 15 different kallikreins (serine type proteases, abbreviated as KLK[1] in reference to the gene, or hK in reference to the protein) (1). Similarly, the mouse and rat kallikrein gene families are characterized by a large number of closely related members that presumably arose because of gene duplication events (2–6). The different members of the mouse and rat kallikreins are characterized by a high degree of amino acid identity, but typically exhibit different preferences toward peptide substrates (7–12). Several human kallikreins have been identified as potentially useful diagnostic markers for breast (KLK3 and KLK6), prostate (KLK2 and KLK3), and ovarian (KLK6, KLK9, KLK10, and KLK11) cancers as well as neurodegenerative diseases such as Alzheimer's (KLK6) (1, 13–17).

Myelencephalon-specific protease (MSP) is a member of the rat kallikrein gene family that is abundantly expressed in the rodent central nervous system and shown to be up-regulated in response to glutamate receptor-mediated excitotoxic injury (18). Potential human homologues to rat MSP have also been identified (18) and have been alternatively named protease M (19), Zyme (20), and neurosin (21). Mouse homologues to MSP have been reported as brain and skin serine protease (BSSP) (22) and brain serine protease (BSP) (23). It has been postulated that MSP/protease M/neurosin may play a key role in the regulation of myelin turnover and in demyelinating disease (18, 24–27), including the development of multiple sclerosis lesions (25). Furthermore, this kallikrein may also play a role in the degradation of β-amyloid or turnover of amyloid precursor protein (28, 29). The kinetic properties of MSP have identified it as a degradative-type protease with broad specificity for cleavage after Arg residues (27). A potential human homologue to rat MSP has been identified (human kallikrein 6, or hK6), based upon amino acid sequence identity (69.1%) in comparison with the other human kallikreins (27, 30). hK6 has the highest expression in the central nervous system, breast, kidney, and uterus and may prove to be a useful biomarker for ovarian and breast cancers as well as Alzheimer's disease (1).

The x-ray crystal structure and biochemical characterization of this enzyme will provide insight into its structure/function relationship and assist in the development of specific inhibitors. We report here biochemical data, phylogenetic analyses, and the x-ray crystal structure for mature active hK6 protein that support its identification as the human homologue to rat MSP and provide a structural interpretation for its catalytic features and autolytic regulation. This report provides the first structural data for one of the human kallikreins, and the x-ray structure determination of hK6 is an important step in elucidating structure/function relationships for this important class of human proteins.

[1] The abbreviations used are: KLK, kallikrein; hK, human kallikrein protein; MSP, myelencephalon-specific protease; MALDI, matrix-assisted laser desorption/ionization; TOF, time of flight; L-BAPNA, benzoyl L-arginine paranitroanilide; AMC, aminomethylcoumarin; MBP, myelin basic protein; PAM, percent accepted mutation; CFAD, complement factor D; r.m.s., root mean square; Tricine, *N*-[2-hydroxy-1,1-bis(hydroxymethyl)ethyl]glycine; BSSP, brain and skin serine protease; BSP, brain serine protease.

EXPERIMENTAL PROCEDURES

Expression, Crystallization, and Data Collection—Mature active hK6 was expressed and purified from a baculovirus/insect cell line system essentially as described for rat MSP (27), using a synthetic Asp$_4$-Lys pro sequence and activation by enterokinase. Purified active hK6 was concentrated to 20 mg/ml in 40 mM sodium acetate, 100 mM NaCl, and 20 mM benzamidine, pH 4.5. Crystallization conditions were identified using a hanging drop sparse matrix screen (31) of precipitants, salts, and pH conditions (Hampton Research, Laguna Niguel, CA). Diffraction quality crystals grew from 30% (w/v) polyethylene glycol 4000, 0.2 M magnesium chloride hexahydrate, and 0.1 M Tris-hydrochloride, pH 8.5, after 2 weeks of incubation at 4 °C.

X-ray intensity data were collected at 103 K from a single crystal ($0.5 \times 0.2 \times 0.05$ mm) with a Rigaku imaging plate area detector R-Axis IIc using Cu-Kα radiation. Data were processed and scaled using DENZO and SCALEPACK (32, 33). This crystal diffracted to at least 1.75 Å. The space group was tentatively identified as orthorhombic P2$_1$2$_1$2$_1$ with cell constants a = 39.1 Å, b = 62.1 Å, c = 85.8 Å. Based upon a molecular mass of ~29 kDa for hK6, a Matthews' coefficient V_m = 1.80 Å^3/Da suggested a single molecule in the asymmetric unit (34).

Molecular Replacement and Structure Refinement—Initial phases were calculated by molecular replacement using Atlantic salmon trypsin (Protein Data Bank code 1A0J) as a search model and the Crystallography and NMR System software package (35). The rotational search resulted in a single peak 8σ above the noise level, and a subsequent translational search in the P2$_1$2$_1$2$_1$ space group of the correctly rotated model resulted in a single peak 4σ above the noise level. The R_{cryst} was 47.3% after rigid body refinement of this initial solution.

A 3-Å 2F_{obs} − F_{calc} SIGMAA-weighted composite annealed omit map (5% of data omitted) was calculated, and the structure was built and refined through alternating cycles using the graphic program *O* (36) and the Crystallography and NMR System software package. All refinements were performed by simulated annealing using a maximum likelihood target, and this cyclic procedure was repeated several times with gradual increase of the resolution to 1.75 Å. A random selection of 3% of the data was assigned for calculation of R_{free} and was not included in the refinement. Solvent molecules were added at the last stage of refinement at stereochemically reasonable positions.

Autolysis of hK6—Autolysis of hK6 was evaluated using 16.5% Tricine SDS-PAGE (37) and activity assays with benzoyl L-arginine paranitroanilide (L-BAPNA). Mature hK6 in phosphate-buffered saline, pH 7.31, was incubated at 37 °C, and samples at time points of 0, 1, 2, 4, 6, 8, 10, and 24 h were taken. Identical samples were evaluated using the L-BAPNA assay and 16.5% Tricine SDS-PAGE. Polypeptides resolved by the Tricine SDS-PAGE were transferred by electroblotting to polyvinylidene difluoride membrane (Bio-Rad) and then subjected to amino-terminal peptide sequencing on an Applied Biosystems Procise 492 model protein sequencer (Applied Biosystems, Foster City, CA).

Determination of Kinetic Constants—Substrate stock solutions of tosyl-Gly-Pro-Arg-aminomethylcoumarin (AMC) and tosyl-Gly-Pro-Lys-AMC (Bachem, King of Prussia, PA) were prepared in Me$_2$SO. Enzyme concentrations of 20 and 200 nM were utilized in the hydrolysis of the Arg- and Lys-containing substrates, respectively. The assay mixture contained 50 mM Tris-HCl and 0.1 mM EDTA, pH 8.5, and the final concentration of Me$_2$SO was less than 5%. Assays were performed using substrate concentrations of 9.0 μM to 2 mM, at 37 °C. Hydrolysis of the AMC substrates was monitored fluorometrically with an excitation wavelength of 380 nm and an emission wavelength of 460 nm on a Varian Cary Eclipse fluorescence spectrophotometer (Varian, Inc., Palo Alto, CA), and all data points were collected in triplicate. Steady-state kinetic constants K_m and k_{cat} were determined from averaged data sets of initial reaction rate *versus* substrate concentration by nonlinear fitting to the Michaelis-Menten equation using the *Datafit* software package (Oakdale Engineering, Oakdale, PA).

Digestion of Myelin Basic Protein and Extracellular Matrix Proteins by hK6—Rat myelin basic protein (MBP) isolated from spinal cord was added to hK6 at a 1000:1 mass ratio in 50 mM Tris and 100 mM NaCl, pH 8.0. This mixture was incubated at 37 °C, and time points were taken at 10, 30, 60, 120, and 240 min. The MBP and degradative fragments were resolved using Tricine SDS-PAGE (16.5%). Laminin from basement membrane of Engelbreth-Holm-Swarm mouse sarcoma (Sigma) was diluted in Tris-buffered saline, pH 7.5, to a concentration of 1 mg/ml. Active hK6 was added to a concentration of 4.2 μM (10:1 (w/w) ratio of laminin/hK6). The sample was incubated at 37 °C, and aliquots of the digestion mix were taken at 0, 1, and 24 h, resolved on 7.5% SDS-PAGE, and visualized by Coomassie Blue staining. Mouse fibronectin (Invitrogen) was used as provided as a stock solution of 1.0

mg/ml in 2.7 mM potassium chloride and 10% glycerol, pH 7.3. Mature hK6 was added to a final concentration of 4.2 μM (10:1 (w/w) ratio of fibronectin/hK6). The sample was incubated at 37 °C, and aliquots were taken and analyzed in a manner identical to that of the laminin digestion.

Phylogenetic Analyses—A data set of hK6-related proteins was collected and assembled from protein sequence databases (as of September 2001) using FastA (38) and LookUp (39) within the Genetics Computer Group's Wisconsin Package SeqLab interface. An expectation value of 10^{-4} was used as a list cut-off, and all entries other than human, rat, and mouse were excluded. Redundancies, splicing variants, and other isoforms were then sorted out, leaving a data set of 33 protein sequences (Table I). PileUp (40) with the BLOSUM30 matrix (41) was used to initially align the sequences, followed by considerable regional realignment and manual adjustment. The final aligned amino acid sequence data set is available from the authors by request.

GCG's ToFastA and Don Gilbert's ReadSeq were used to create a PHYLIP (42) format data set from the alignment, where columns of excessive homoplasy, as judged by similarity less than 15%, were excluded. Three phylogenetic inference methods were used on the resultant data matrix. 1) The maximum likelihood, quartet-puzzling program Tree-Puzzle (43) run with the JTT amino acid substitution model (44) and 1000 steps produced a maximum likelihood tree estimate with branch lengths and node support values. 2) Pairwise distances were estimated with PHYLIP's ProtDist PAM model (45) and least squares fit to an optimal globally rearranged tree by the PHYLIP Fitch algorithm with 10 random additions. 3) The data matrix was bootstrapped 100 times by PHYLIP's SeqBoot, ProtDist generated 100 PAM-based pairwise distance matrices, and then PHYLIP's Neighbor neighbor-joining algorithm and Consense program provided bootstrap node support values. Majority rule (*i.e.* wherever two or more of the three estimates agreed) provided the resolved clades on the final tree presented in Fig. 1. Final node supports values were calculated as the average between the Tree-Puzzle and bootstrapped neighbor-joining results wherever they agreed on a particular node; all values greater than 50% were printed at their respective node.

TABLE I
Sequences in phylogenetic analysis
Gene symbols without organism identifiers are all from humans, and all sequences are in same order as in Fig. 1.

Gene	other names	NCBI GI designation	GenBank accession
KLK10	breast normal epithelial, PRSSL1, NES1	10799395, 11244768, 3065711	AC011473, AF243527, AF055481, AF024605
KLK12	KLKL5	6249632, 6166249, 10799397, 11244770	AF135025, AC011473, AF243527
KLK2	glandular kallikrein 1	386842, 7527776, 6425046, 4261522, 11244761	M18157, AC037199, AF188746, S39329, AF243527
KLK13	KLKL4	6063386, 10799398	AF135024, AC011473
KLK14	KLKL6	6715552, 10799399	AF161221, AC011473
KLK15	ACO protease	9957760, 11244759	AF242195, AF243527
KLK5	KLKL2, SCTE, stratum corneum tryptic-like	4589283, 6063033, 11244763	AF135028, AF168768, AF243527
KLK4	KLKL1, PRSS17, enamel matrix serine protease, prostase	8896096, 11244762, 7920367, 6136038, 4589272, 5020095, 5020096, 9926920, 4512029, 4512030, 4512031, 4512032, 9296995	AF259969, AF243527, AF228497, AF135023, AF113140, AF113141, AF148532, AAD21580, AAD21581, AAD38019
	mouse prostase	9230643, 4090847	AF198031, AF019979
KLK7	PRSS6, SCCE, stratum corneum chymotrypsin	2297543, 532504, 5733684, 11244765	L33404, A42048, AF166330, AF243527
	mouse stratum corneum	6010462	AF124299
CFAD	complement factor D, adipsin, EVE	178625, 15131535	M84526, AJ313463
	rat CFAD	693722	S73894
	mouse CFAD	202167, 673431	M11768, X04673
	rat trypsin V	57413, 57415	X59012, X59013
TRP1	trypsin I, PRSS1, TRY1	1552515, 521216	M22612
	trypsin II PRSS2, TRY2, anionic trypsinogen E	521218, 1552517, 2275595	M27602
	trypsin III PRSS3, TRY3	37460	X15505
	trypsin IV PRSS4, TRY4	464951, 6066378, 3980129	X72781, X71345
	rat trypsin I	57408, 206508	J00778, V01273
	rat trypsin II	758266, 206506	V01274, L00130, L00131
	mouse trypsin II	54919, 4239961, 2358119	X04574, AB017030
	rat trypsin III, cationic	206499	M16624
	rat trypsin IV	56814, 2358083	X15679
KLK9	KLKL3	5919239, 10765093, 10799394, 11244767	AF135026, AC011473, AF243527
KLK11	PRSS20, TLSP, hippostasin, prostate-type hippostasin, keratinocyte trypsin-like protease	5713131, 6681454, 9296987, 8574439, 3649791, 10799396, 11244769	AF164623, AB013730, AB041036, AB012917, AC011473, AF243527
	mouse hippostasin	6681653	AB016226
KLK8	PRSS19, NRPN, BSP1, TADG14, neuropsin, ovasin	3176387, 4768607, 5672473, 5672479, 5918518, 11244766	AB009849, AF095743, AB008390, AB008927, AF055982, AF243527
	rat neuropsin	3559978	AJ005641
	mouse neuropsin	1020091, 7229069	D30785, AB032202
KLK6	PRSS9, protease M, zyme, neurosin, myelencephalon specific protease	1518788, 1505493, 2318115, 5791636, 11244764	U62801, D78203, E13202, I95869, AF013988, AF149289, AF243527
	rat MSP	2853366	AF016269
	mouse MSP, BSSP, BSP	3241912, 4220546, 5913973	AB015206, Y18723, AB032402

FIG. 1. **Majority rule consensus tree (modified from TreeView (62) output) of three phylogenetic inference estimates from protein sequence.** Horizontal branch length is proportional to evolutionary divergence in units of substitutions per site according to the *scale bar* at the *bottom*, whereas nothing is implied by vertical order. Node support values greater than 50% are printed at appropriate nodes and are an average of Tree-Puzzle and bootstrapped neighbor-joining support values. Human sequences are only labeled with gene/protein identifiers; rodent sequences are labeled as mouse or rat along with the gene identifier.

RESULTS

Recombinant hK6 Protein—The homogeneity of purified hK6 was evaluated using amino-terminal sequencing and MALDI-TOF mass spectrometry. Mass spectrometry revealed that the hK6 samples used for crystallization contained intact, glycosylated enzyme (Fig. 2). The major peak had a mass of 25,866 Da, which is a difference of +1366 Da from the mass calculated from the protein sequence. This extra mass corresponds to approximately six *N*-acetylglucosamine molecules. Furthermore, peaks corresponding to six different glycosylated forms were visible in the mass spectrum, with the average difference in mass between each form being ~184 Da (corresponding to the mass of one hexose unit). Amino-terminal sequencing analysis yielded a single sequence of Leu-Val-His-Gly, representing the correct amino-terminal sequence for mature hK6.

X-ray Structure Refinement—A total of 140 solvent molecules were added to the refined hK6 structure. One tentatively assigned solvent molecule exhibited octahedral coordination geometry with adjacent solvent molecules and short (~2.0 Å) contact distances with these groups. This solvent was therefore assigned as a Mg^{2+} ion (46). Unambiguous density was also

visible within the active site region, indicating the presence of a bound benzamidine inhibitor with terminal amine groups clearly defined. In the final refined structure, 227 of the 229 amino acid residues are defined in the electron density map. The observed electron density is in full agreement with the amino acid sequence deduced from the cDNA sequence (20). The peptide backbone of hK6 could be traced unambiguously from its amino-terminal Ile^{16} to Gln^{243} (using the chymotrypsinogen numbering scheme (47)). C-terminal residues Ala^{244} and Lys^{245} lacked adequate electron density and were not built into the model. The side chain residues of Lys^{24}, Arg^{110}, Gln^{239}, and Gln^{243} are undefined in the electron density map and were therefore modeled as Ala residues. Asp^{150} was modeled in multiple rotamer conformations. Some of the loop regions, in particular the region from Trp^{215} to Pro^{225}, required extensive rebuilding due to large differences from that of the search model. The model refined to acceptable values of stereochemistry and crystallographic residual (Table II).

Digestion of Myelin-related and Extracellular Matrix Proteins by hK6—Rat MBP was extensively and rapidly degraded by hK6 (Fig. 3). Extended incubation resulted in a characteristic pattern of four lower molecular mass fragments. Rat plasma fibronectin was rapidly degraded by hK6 to yield a polypeptide with an apparent molecular mass of ~200 kDa (Fig. 3). This polypeptide was subsequently degraded to numerous smaller fragments after extended incubation with hK6. Mouse laminin was likewise rapidly degraded by hK6, yielding an initial polypeptide with a mass of ~140 kDa and numerous smaller peptide fragments (Fig. 3).

Determination of Steady-state Kinetic Constants—Active hK6 exhibited characteristic Michaelis-Menten kinetics with all substrates. Kinetic constants for the hydrolysis of tosyl-Gly-Pro-Arg-AMC and tosyl-Gly-Pro-Lys-AMC are listed in Table III. When compared with rat MSP, hK6 has a somewhat reduced activity toward these substrates and exhibits a general preference in k_{cat} for Arg in the substrate P1 position relative to Lys.

Autolysis of hK6—Tricine SDS-PAGE revealed that hK6 undergoes autolysis (Fig. 4). Amino-terminal sequencing of the Tricine SDS-PAGE-resolved autolysis fragments identified a peptide sequence corresponding to a single cleavage site between residues Arg^{76} and Glu^{77}. Activity assays against L-BAPNA indicate that the autolytic event results in a corresponding loss of enzyme activity and that this autolytic inactivation follows a second order rate constant (data not shown).

Phylogenetic Analyses—The three phylogenetic inference estimations consistently grouped certain clades, yet the resolution at the base of the tree remained obscure. Importantly, every analysis specifically associated human hK6 with the rodent MSPs, clearly indicating their orthologous relationship. This particular node on the tree had almost as much support as that grouping the rat and mouse MSPs to each other, 83.5 and 89.5%, respectively. Other orthologues between the human and rodent genes in the tree were as expected and range in support value from below 50% for the hK4 human and mouse homologues to 98% in the human and mouse hK7 system. Paralogous hK relationships in the tree, where they were resolved, had quite low support values, ranging from below 50% for those nodes associating hK7 with hK5 and hK4 to 62% between hK2 and hK13 and up to 73.5% between hK9 and hK11. Conversely, the support values for most of the classical trypsin homologues were quite high, although the complement factor D (CFAD) system is only weakly supported, at 53%, as being trypsin's nearest paralogue. hK10 appeared to have diverged the furthest from the common ancestor of all the hKs, although hK15
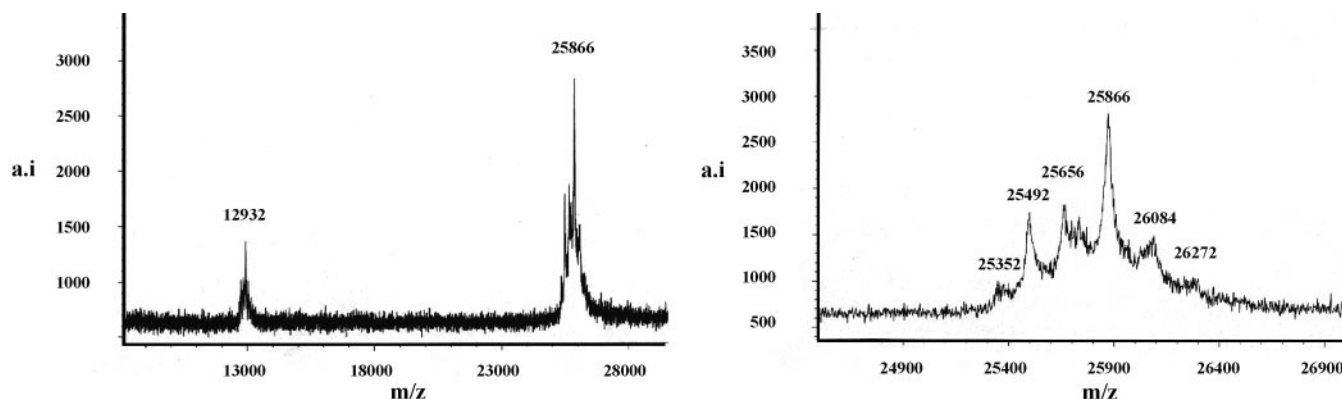
Fig. 2. *Left panel*, MALDI-TOF mass spectrum of purified, active recombinant hK6, with an indicated mass of 25.866 kDa (also shown is a peak at 12.932 kDa that represents intact hK6 at one-half the m/z ratio). *Right panel*, enlarged view of the peak at 25.866 kDa showing the presence of six forms. The average difference in molecular mass between each peak is 184 Da, or 1 hexose unit, indicating that the mass heterogeneity is related to heterogeneity of glycosylation.

TABLE II
Crystal, data collection, and refinement statistics

Parameter	Value
Crystal data	
Space group	$P2_12_12_1$
Cell dimensions (Å)	$a = 39.1$, $b = 62.1$, $c = 85.8$
Molecules/asymmetric unit	1
Matthews' constant (V_m) (Å³/Da)	1.80
Maximum resolution (Å)	1.75
Data Collection and Processing	
Total/unique reflections	495,027/21,777
Completion (43–1.75 Å)/(1.79–1.75 Å) (%)	96.0/82.7
I/σ (43–1.75 Å)/(1.79–1.75 Å)	43.0/4.9
R_{merge} (43–1.75 Å)/(1.79–1.75 Å) (%)	5.7/38.2
Wilson temperature factor (Å²)	26.6
Refinement	
R_{cryst} (43–1.75 Å) (%)	20.9
R_{free} (43–1.75 Å) (%)	24.1
r.m.s. bond length deviation (Å)	0.005
r.m.s. bond angle deviation (degrees)	1.35
r.m.s. B-factor deviation (σ)	2.83
Ramachandran plot (%)	
Most favored region	87.6
Additional allowed region	12.4
Generously allowed region	0
Disallowed region	0
Number of atoms/molecule	
Non-H protein	1,685
Water/ion	139/1
Average thermal factors (Å²)	
All atoms	30.9
Protein atoms	30.3
Solvent molecules	27.7
Benzamidine	32.0

and hK4 were almost as divergent. All of the trypsins and CFADs diverged as much or greater from the common ancestor of all of the sequences on the tree as did any of the hKs. In fact, the human CFAD had almost 0.7 substitutions per site along its length in its divergence from the last common ancestor of the data set.

DISCUSSION

Human Kallikrein 6 Is Functionally Related to Rat MSP—Previously reported Northern blot analysis of rat MSP and KLK6 has demonstrated a similar abundant expression in the brain in comparison with peripheral tissues (48). These studies also demonstrated tissue-specific expression in the spinal cord and medulla oblongata and showed that the pattern of expression of MSP differed from that of tissue plasminogen activator. Rat MSP exhibits the highest amino acid identity (69.1%) with hK6, in comparison with the other human kallikreins; KLK6

has therefore been proposed as the human homologue of MSP (27). The present phylogenetic analysis strongly corroborates this assertion. Despite basal resolution so poor that it is impossible to tell with any confidence just what the ancestral paralogous branching order of the kallikreins was, the orthology of hK6 and the rodent MSPs is obvious (with nearly 85% node support value). Future work in pursuing these basal relationships is being done through the use of a DNA alignment that corresponds to our aligned protein data set. Much more sophisticated models of evolution are available for DNA than for protein data sets, especially as implemented in the PAUP* (49) maximum likelihood method. These sophisticated models may provide a greater evolutionary look-back time than the present study achieved and allow for the teasing of some order out of the original gene duplications that led to this large, complicated, and important gene family.

Rat MSP is characterized as a degradative protease, with greater catalytic efficiency for Arg *versus* Lys in the P1 position. It has been shown to rapidly degrade various myelin-associated and extracellular matrix proteins and is autolytically regulated via cleavage after residue positions Arg[74] and Arg[81] (27). The results of the present study demonstrate that the characteristic digestive patterns exhibited by hK6 against MBP, laminin, and fibronectin substrates are virtually identical to those seen with rat MSP (27). Rat MSP and hK6 are also both inactivated by autolysis; however, the sites of autolysis are similar but not identical. Arg residues are present at positions 74 in both hK6 and rat MSP; however, whereas rat MSP has an Arg at position 81, hK6 has a Glu. Conversely, while hK6 has an Arg at position 76, rat MSP has a Thr. Therefore, when considering the arginine preference of both enzymes, hK6 could autolytically cleave at positions 74 and 76, whereas rat MSP could cleave at positions 74 and 81. Whereas positions 74 and 81 in rat MSP are autolytically cleaved, amino-terminal sequencing of autolyzed hK6 identifies only an amino terminus starting at residue position 76. It may be the case that hydrolysis after arginine 76 occurs rapidly in hK6, and therefore subsequent hydrolysis after arginine 74 releases a dipeptide that would be lost during PAGE resolution. In any event, the data indicate that for both hK6 and rat MSP, autolytic cleavage in the region 74–76 results in inactivation of the enzyme. Thus, with regard to enzymatic activity toward myelin-related and extracellular proteins and autolytic properties, hK6 and rat MSP appear to be true functional homologues. The ability of both rat MSP and hK6 to degrade myelin-associated proteins, coupled with data showing that this enzyme is abundantly expressed within inflammatory cells at sites of demyelination

Structure and Biochemical Properties of hK6
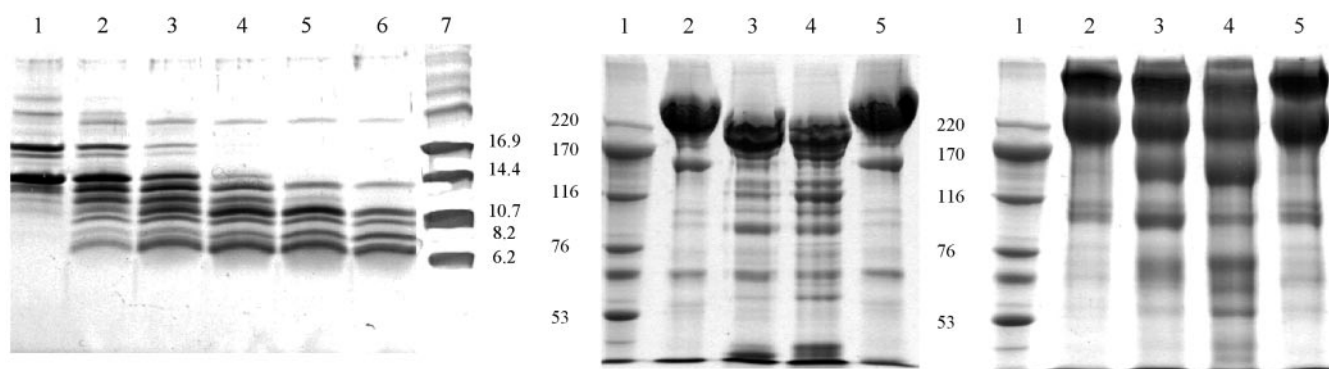
FIG. 3. *Left panel*, degradation of MBP by hK6 (see "Experimental Procedures" for details). *Lane 1*, control with no added hK6; *lane 2*, 10-min incubation; *lane 3*, 30 min; *lane 4*, 60 min; *lane 5*, 2 h; *lane 6*, 4 h; *lane 7*, molecular mass markers. *Middle panel*, 7.5% SDS-PAGE (reducing) showing digestion of fibronectin by hK6 at 37 °C in 2.7 mM KCl, 340 mM NaCl, 8 mM sodium phosphate, 1.5 mM potassium phosphate, and 10% glycerol, pH 7.3. *Lane 1*, molecular mass markers; *lane 2*, fibronectin + hK6, 0 h; *lane 3*, fibronectin + hK6, 1 h; *lane 4*, fibronectin + hK6, 24 h; *lane 5*, fibronectin control, 24 h. *Right panel*, 7.5% SDS-PAGE (reducing) showing digestion of laminin by hK6. *Lane 1*, molecular mass markers; *lane 2*, laminin + hK6, 0 h; *lane 3*, laminin + hK6, 1 h; *lane 4*, laminin + hK6, 24 h; *lane 5*, laminin control, 24 h.

TABLE III
Kinetic constants for hydrolysis of Tosyl-Gly-Pro-Arg-AMC and Tosyl-Gly-Pro-Lys-AMC substrates by mature hK6
(50 mM Tris, 0.1 mM EDTA, 4% Me$_2$SO, pH 8.5, 37 °C)

Substrate	$k_{cat}(s^{-1})$	$K_m(\mu M)$	k_{cat}/K_m ($M^{-1} s^{-1}$)
hK6			
Tosyl-Gly-Pro-Arg-AMC	6.84 ± 0.79	1562 ± 266	4.40 ± 0.30 × 10^3
Tosyl-Gly-Pro-Lys-AMC	0.026 ± 0.004	777 ± 181	3.30 ± 0.20 × 10^1
rMsp[a]			
Tosyl-Gly-Pro-Arg-AMC	14.4 ± 0.40	408 ± 19	3.53 ± 0.08 × 10^4
Tosyl-Gly-Pro-Lys-AMC	0.13 ± 0.01	269 ± 10	4.80 ± 0.10 × 10^2
Bovine trypsin I[b]			
Tosyl-Gly-Pro-Arg-AMC	29.0 ± 1.0	3.5 ± 0.5	9.00 ± 1.0 × 10^6
Tosyl-Gly-Pro-Lys-AMC	16.9 ± 0.08	12.3 ± 1.2	1.36 ± 0.05 × 10^6

[a] Values from Ref. 27.
[b] Values from Ref. 63.
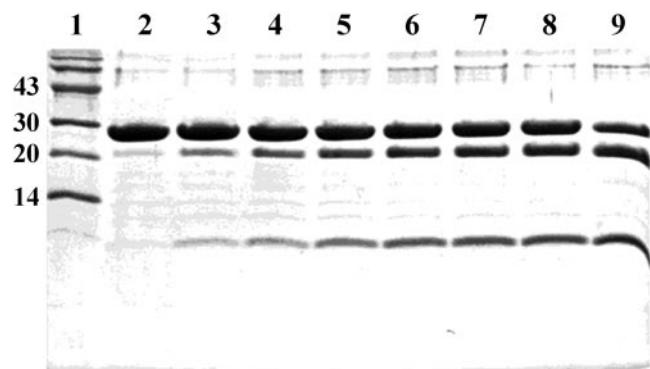
FIG. 4. **Autolysis of hK6 (see "Experimental Procedures" for details).** *Lane 1*, molecular mass markers; *lane 2*, purified active hK6 at zero time point; *lane 3*, 1 h; *lane 4*, 2 h; *lane 5*, 4 h; *lane 6*, 6 h; *lane 7*, 8 h; *lane 8*, 10 h; *lane 9*, 24 h.

in murine models of multiple sclerosis and associated lesions, supports the idea that this enzyme may play a pivotal role in demyelinating disease (18, 26, 27, 50).

Autolytic Activity of hK6—Determination of the x-ray structure of hK6 provides an opportunity to further characterize the autolytic regulation of MSP/hK6. Unlike the mouse kallikreins, and similar to trypsin, autolysis of hK6 leads to inactivation. Thus, autolysis represents a potential regulatory mechanism in controlling the activity of hK6. The locations of the autolytic sites of hK6, in juxtaposition to the active site region, are shown in Fig. 5. Not surprisingly, Arg[76] (a site of autolysis in hK6) is the most solvent-accessible arginine residue in the structure. Although the sites of autolysis in hK6 and trypsin are not identical, both proteases autolyze within the amino-

terminal domain (Fig. 5). The two canonical sites of autolysis in the mouse kallikreins, which are not associated with inactivation (51, 52), are located within the extended kallikrein loop at position 95 and within the carboxyl-terminal domain at position 148 (Fig. 5). Cleavages at the locations within the amino-terminal domain in trypsin and hK6 may result in destabilization of the structure, and inactivation by autolysis may represent a stability-based mechanism of inactivation. The autolytic properties of the regulatory protease thrombin provide another contrast to hK6. Thrombin contains Arg residues at positions 73 and 75. Autolysis at these positions in thrombin does not result in inactivation; rather, it affects substrate specificity (abolishing the specificity for fibrinogen) (53). Since autolysis in hK6 abolishes catalytic activity, the autolytic properties of hK6 are more similar to the digestive enzyme trypsin than to thrombin.

The natural pro-peptide sequence of hK6 is Glu-Glu-Gln-Asn-Lys (19), and cleavage after the Lys residue produces mature active hK6. Rat MSP has a similar activation pro-peptide sequence of Glu-Asp-Gln-Asp-Lys (48) and is not activated by autolytic digestion (27). This inability of rat MSP to self-activate has led to the proposal that a distinct, Lys-specific protease is responsible for activation of rat MSP *in vivo* (27). Similarly, the preference for cleavage after Arg *versus* Lys residues in the P1 position suggests that a distinct Lys-specific protease is hypothesized to activate pro-hK6 *in vivo*.

Overall Structural Relationship of hK6 with Other Serine Proteases—The secondary structure of hK6 is composed of 13 β-strands, two α-helices, two 3$_{10}$-helices, and eight identifiable loop regions. These loop regions have varying functions that, based upon the structures of related serine proteases, include defining substrate specificity (54–57) and autolytic regulation (27, 58, 59). In addition, these loops can provide sites for *N*-
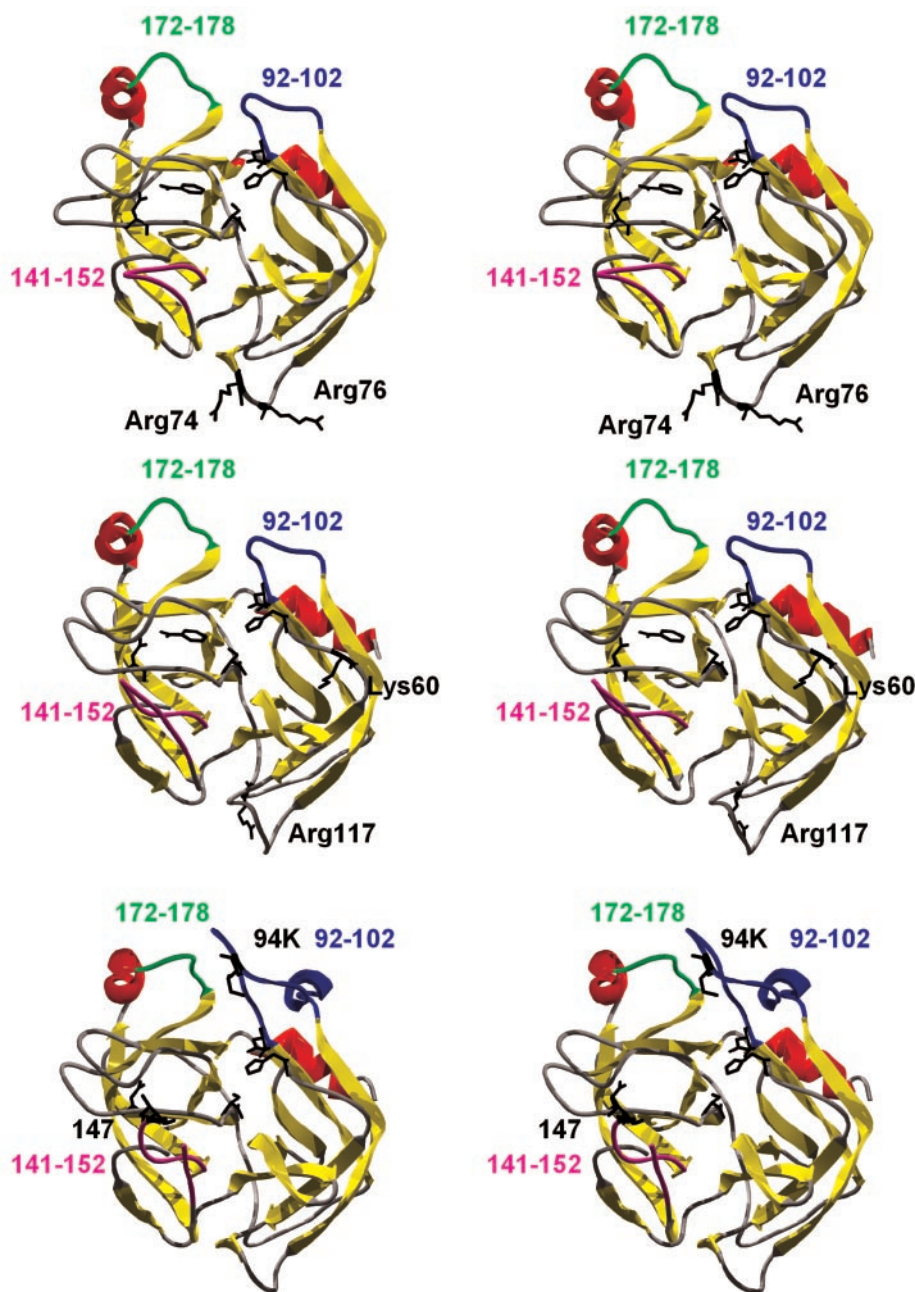
FIG. 5. **Relaxed stereo ribbon diagrams of hK6 (*top panel*), bovine trypsin (1CE5; *middle panel*), and mouse glandular kallikrein 13 (*mK13*) (1AO5; *lower panel*).** Orientation is intended to show the active site cleft with locations of catalytic triad (His^{57}, Asp^{102}, and Ser^{195}), S1 site (Asp^{192}), and bound benzamidine inhibitor (if present). Also indicated are the locations of the autolysis sites in hK6 and bovine trypsin. The two canonical autolysis sites in the mouse kallikreins are indicated using the structure of mK13. Also shown are the locations of the loop regions 92–102 (*blue*), 141–152 (*magenta*), and 172–178 (*green*) that border the active site.

glycosylation that may serve to regulate activity in this class of enzyme (60).

The overall structure of hK6 is more similar to that of bovine trypsin than the mouse kallikrein mK13 (prorenin-converting enzyme, one of the few available mouse kallikrein structures), and the superimposed structures have r.m.s. deviations of 0.79 and 1.06 Å, respectively. When comparing the x-ray structure of hK6 with either bovine trypsin or mK13, there are three immediately identifiable loop regions adjacent to the active site that exhibit structural heterogeneity. These include residue positions 91–103 (the "kallikrein loop"), 141–152, and 172–178 (Fig. 5). The "kallikrein loop" is a sequence of up to 11 amino acids inserted between the sixth and seventh β-sheets (after residue 94) in the kallikrein family of enzymes. hK6 has no inserted residues in this region and thus lacks the classical kallikrein loop. This loop in hK6 is indistinguishable in length in comparison with the degradative proteases trypsin and chymotrypsin and is shorter than that seen in mouse kallikreins or other regulatory type proteases (Fig. 6). Although the amino

acid sequences within this region differ between hK6 and trypsin, the structures are essentially identical (Figs. 5 and 6).

The short surface loop comprising residue positions 172–178 is identical in length for the different proteases compared in Fig. 6. The amino acid sequence for hK6 within this region is identical to that of bovine trypsin with the exception of position 178 (Fig. 6) and adopts a structure essentially identical to that of bovine trypsin (Fig. 5). This short loop is oriented away from the active site, and contrasts with the homologous region in mK13, which is oriented toward the active site (Fig. 5).

The loop region 141–152 in hK6 is shorter than that in trypsin (Fig. 6) and leads to a conformation that orients this loop away from the active site in comparison with trypsin (Fig. 5). In the comparison with other proteases (Fig. 6), the broad specificity degradative proteases generally have a shorter length loop in this region, whereas the regulatory proteases have longer loops that afford more extensive structural determinants of the substrate binding site.

The structural data for the variable surface loop regions that

border the active site of hK6 describe loops that are both short and generally oriented away from the substrate binding site. Thus, their contribution to formation of the S2 and S3 sites within the protease appears limited. This is a characteristic feature of the degradative type proteases, exemplified by the digestive enzymes trypsin and chymotrypsin (61). Thus, the original hypothesis (18) that rat MSP is a trypsin-like digestive enzyme expressed in the central nervous system, is supported by both the enzymatic properties of MSP (27) and the biochemical and structural data reported here for the human homo-

logue hK6. The activity of hK6 toward small peptide substrates indicates relatively large values for K_m (Table III). This apparently weak binding affinity may reflect limited interactions within the S2 and S3 sites, as is suggested from the general structural data of the active site. Thus, hK6 may function effectively only with larger peptide substrates with the potential for extended contact interactions beyond the S2 and S3 sites. The rapid digestion of myelin basic protein is consistent with this hypothesis.

S1 Site Structural Features—Residues 189–195, 214–220, and 224–228, in addition to the catalytic triad, define the S1 binding pocket. The presence of a bound benzamidine inhibitor in the x-ray structure of hK6 permits an evaluation of how the guanidino group of a substrate P1 Arg side chain might fit within the active site. In trypsin, each of the nitrogen groups of the bound benzamidine inhibitor hydrogen-bonds to an oxygen moiety of the Asp[189] in the "bottom" of the S1 binding pocket (Fig. 7). In porcine kallikrein (an available kallikrein structure with a bound benzamidine inhibitor), the Oγ moiety of the Ser side chain at position 226 displaces one of the benzamidine amide groups and forces a rotation of the benzamidine ring of $\sim$60° away from the Ser side chain (61). Similar to trypsin, hK6 has a Gly residue at position 226, and the interaction of benzamidine with the Asp[189] side chain is virtually indistinguishable from that of trypsin (1CE5) and distinctly different from the orientation in porcine kallikrein (2PKA) (Fig. 7).

Further structural similarity of the S1 site between hK6 and trypsin is achieved due to structural changes within the local region 215–220. This region in trypsin adopts a conformation that results in a hydrogen bonding interaction between the main chain carbonyl of residue Gly[218] with a benzamidine

```
                  94 A B C D E F G H I J K         100
hK6            P D Y - - - - - - - - - - D A A S H D Q D
rMSP           P R Y - - - - - - - - - - N P Q T H D N D
Trypsin (1CE5) P S Y - - - - - - - - - - N S N T L N N D
Chymotrypsin (2GCH) S K Y - - - - - - - - - - N S L T I N N D
mK13 (1AO5)    P G F N M S L L M L Q T I P P G A D F S D D
Neuropsin (1NPM) P C Y N - - - - - - - N S N P E D H S H D
ppKA (2PKA)    P G F N L - - - - - - - S A D G K D Y S H D

                  144 A B C G H I    147 152
hK6            W G K T A - - - - D G D F P
rMSP           W G K M E - - - - N G E F P
Trypsin (1CE5) W G N T K S - - S G T S Y P
Chymotrypsin (2GCH) W G L T - - - - - - R Y T P
mK13 (1AO5)    W G S I T - - - P T W Q K P
Neuropsin (1NPM) W G T V T S - - P Q E N F P
ppKA (2PKA)    W G S I E P G P D D F E F P

                  175            215      222 A      230
hK6            Y P G Q I T Q   S W G N I P C G S K E K P G V Y T N
rMSP           Y P G K I T R   S W G D M P C G S K E K P G V Y T D
Trypsin (1CE5) Y P G I T S   S W G - S G C A Q K N K P G V Y T K
Chymotrypsin (2GCH) W G T K I K D S W G S S T C S T - S T P G V Y A R
mK13 (1AO5)    Y L Q K V T D   S Y G P V P C G K P G V P A I Y T N
Neuropsin (1NPM) Y P G K I T E S W G S D P C G K P E K P G V Y T K
ppKA (2PKA)    H P D K V T E   S W G H T P C G S A N K P S I Y T K
```

FIG. 6. **X-ray structure-based alignment of the primary sequence of the loop regions 92–102, 141–152, 172–178, and 214–230 for hK6, MSP, trypsin, chymotrypsin, mouse kallikrein 13, neuropsin, and porcine kallikrein (Protein Data Bank accession codes are given).**

FIG. 7. **Relaxed stereo diagram showing details of the S1 binding pocket in hK6 (*upper panel*), bovine trypsin (1CE5; *middle panel*), and porcine kallikrein (2PKA, *lower panel*).** The hydrogen bonding interactions of the bound benzamidine inhibitor are shown using *broken lines* (residue positions 191–193 are omitted for clarity).
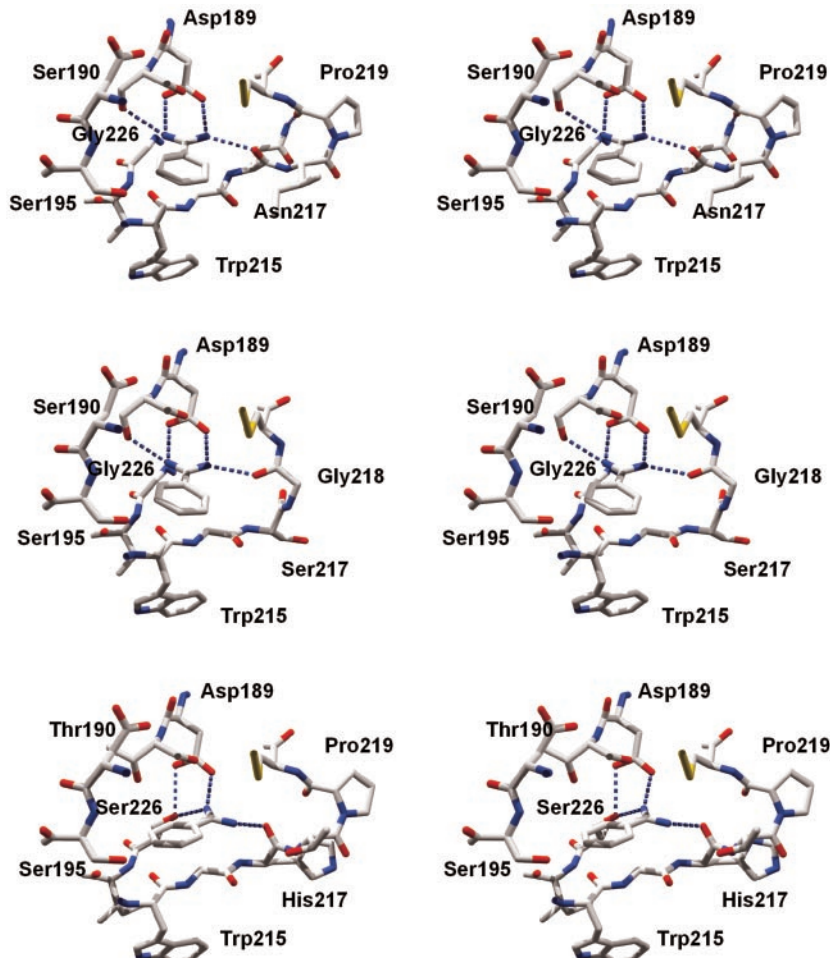
nitrogen group (Fig. 7). Although region 215–220 in hK6 has an amino acid insertion in comparison with the same region in trypsin, it adopts a conformation that positions the main chain carbonyl of residue Asn[217] in an almost identical location to that of Gly[218] in trypsin (Fig. 7). Although region 215–220 in porcine kallikrein has the same length as in hK6, there are slight conformational changes, presumably in response to the Ser[226] residue. These conformational changes position the main chain carbonyl of residue 217 further away from the bound benzamidine and permit a hydrogen bonding interaction with the alternatively oriented benzamidine nitrogen (Fig. 7). These structural features in hK6 suggest a generally optimized fit for a P1 guanidino group within the active site that translates into a much higher catalytic efficiency toward substrates with an Arg *versus* Lys residue in this position.

Site of Glycosylation—It has been reported that *N*-linked oligosaccharides within the "kallikrein loop" of neuropsin (the apparent mouse homologue of KLK8) affect the size of the S2 pocket and that mutations in this region result in a significant decrease in both k_{cat} and K_m (while maintaining the overall k_{cat}/K_m) (60). As previously mentioned, hK6 lacks the equivalent kallikrein loop characteristic of the regulatory proteases, including the *N*-linked Asn residue at position 95 (Fig. 6). However, mass spectrometry data suggest that there is a potential *N*-linked glycosylation site (sequence Asn-Xaa-Thr) at position Asn[132] that is not present in any of the other known kallikrein structures. In contrast to the *N*-glycosylation site found on the kallikrein loop in other kallikreins, residue 132 is quite distant from the active site and lies at the "rear" of the enzyme. There is electron density present in this region that is indicative of possible sugar residues, but the density is not sufficient for accurate modeling. The function of this site of glycosylation has yet to be determined, but due to its distal location from the active site it is hypothesized not to significantly affect enzyme specificity or function.

In conclusion, the present study provides biochemical and phylogenetic data to support the identification of hK6 as the homologue of rat MSP. The biochemical and structural data also support the original hypothesis by Isackson and co-workers (18) that the MSP/KLK6 gene codes for a trypsin-like degradative protease that is expressed in the brain. Since our recent studies implicate excess MSP/hK6 activity in the development of immune mediated demyelination in both animal models of multiple sclerosis and in human multiple sclerosis lesions (27, 50), the availability of an atomic model of mature hK6, reported herein, may prove useful in the design of specific and potentially therapeutic inhibitors of this unique enzyme.

REFERENCES

1. Yousef, G. M., and Diamandis, E. P. (2001) *Endocr. Rev.* **22,** 184–204
2. Evans, B. A., Drinkwater, C. C., and Richards, R. I. (1987) *J. Biol. Chem.* **262,** 8027–8034
3. Mason, A. J., Evans, B. A., Cox, D. R., Shine, J., and Richards, R. I. (1983) *Nature* **303,** 300–307
4. Wines, D. R., Brady, J. M., Pritchett, D. B., Roberts, J. L., and MacDonald, R. J. (1989) *J. Biol. Chem.* **264,** 7653–7662
5. Wines, D. R., Brady, J. M., Southard, E. M., and MacDonald, R. J. (1991) *J. Mol. Evol.* **32,** 476–492
6. Gerald, W. L., Chao, J., and Chao, L. (1986) *Biochim. Biophys. Acta* **866,** 1–14
7. Blaber, M., Isackson, P. J., James C. Marsters, J., Burnier, J. P., and Bradshaw, R. A. (1989) *Biochemistry* **28,** 7813–7819
8. Frey, P., Forand, R., Maciag, T., and Shooter, E. M. (1979) *Proc. Natl. Acad. Sci. U. S. A.* **76,** 6294–6298
9. Hosoi, K., Tsunasawa, S., Kuihara, K., Aoyama, H., Ueha, T., Murai, T., and Sakyama, F. (1994) *J. Biochem.* (*Tokyo*) **115,** 137–143
10. Jongstra-Bilen, J., Coblenz, L., and Shooter, E. M. (1989) *Brain Res. Mol. Brain Res.* **5,** 159–169
11. Kim, W.-S., Nakayama, K., Nakagawa, T., Kawamura, Y., Haraguchi, K., and Murakami, K. (1991) *J. Biol. Chem.* **266,** 19283–19287
12. Wilson, W. H., and Shooter, E. M. (1979) *J. Biol. Chem.* **254,** 6002–6009
13. Diamandis, E. P., Okui, A., Mitsui, S., Luo, L. Y., Soosaipillai, A., Grass, L., Nakamura, T., Howarth, D. J., and Yamaguchi, N. (2002) *Cancer Res.* **62,** 295–300
14. Yousef, G. M., Kyriakopoulou, L. G., Scorilas, A., Fracchioli, S., Ghiringhello, B., Zarghooni, M., Chang, A., Diamandis, M., Giardina, G., Hartwick, W. J., Richiardi, G., Massobrio, M., Diamandis, E. P., and Katsaros, D. (2001) *Cancer Res.* **61,** 7811–7818
15. Diamandis, E. P., Yousef, G. M., Petraki, C., and Soosaipillai, A. R. (2000) *Clin. Biochem.* **33,** 663–667
16. Diamandis, E. P., Yousef, G. M., Soosaipillai, A. R., and Bunting, P. (2000) *Clin. Biochem.* **33,** 579–583
17. Luo, L. Y., Bunting, P., Scorilas, A., and Diamandis, E. P. (2001) *Clin. Chim. Acta* **306,** 111–118
18. Scarisbrick, I. A., Towner, M. D., and Isackson, P. J. (1997) *J. Neurosci.* **17,** 8156–8168
19. Anisowicz, A., Sotiropoulou, G., Stenman, G., Mok, S. C., and Sager, R. (1996) *Mol. Med.* **2,** 624–636
20. Little, S. P., Dixon, E. P., Norris, F., Buckley, W., Becker, G. W., Johnson, M., Dobbins, J. R., Wyrick, T., Miller, J. R., MacKellar, W., Hepburn, D., Corvalan, J., McClure, D., Liu, X., Stephenson, D., Clemens, J., and Johnstone, E. M. (1997) *J. Biol. Chem.* **272,** 25135–25142
21. Yamashiro, K., Tsuruoka, N., Kodama, S., Tsujimoto, M., Yamamura, Y., Tanaka, T., Nakazato, H., and Yamaguchi, N. (1997) *Biochim. Biophys. Acta* **1350,** 11–14
22. Meier, N., Dear, T. N., and Boehm, T. (1999) *Biochem. Biophys. Res. Commun.* **258,** 374–378
23. Matsui, H., Kimura, A., Yamashiki, N., Moriyama, A., Kaya, M., Yoshida, I., Takagi, N., and Takahashi, T. (2000) *J. Biol. Chem.* **275,** 11050–11057
24. Yamanaka, H., He, X., Matsumoto, K., Shiosaka, S., and Yoshida, S. (1999) *Mol. Brain Res.* **71,** 217–224
25. Scarisbrick, I. A., Asakura, K., Blaber, S., Blaber, M., Isackson, P. J., Bieto, T., Rodriguez, M., and Windebank, A. J. (2000) *Glia* **30,** 219–230
26. Scarisbrick, I., Isackson, P. J., Ciric, B., Windebank, A. J., and Rodriguez, M. (2001) *J. Comp. Neurol.* **431,** 347–361
27. Blaber, S. I., Scarisbrick, I. A., Bernett, M. J., Dhanarajan, P., Seavy, M. A., Jin, Y., Schwartz, M. A., Rodriguez, M., and Blaber, M. (2002) *Biochemistry* **41,** 1165–1173
28. Ogawa, K., Yamada, T., Tsujioka, Y., Taguchi, J., Takahashi, M., Tsuboi, Y., Fujino, Y., Nakajima, M., Yamagoto, T., Akatsu, H., Mitsui, S., and Yamaguchi, N. (2000) *Psych. Clin. Neurosci.* **54,** 419–426
29. Diamandis, E. P., Yousef, G. M., Soosaipillai, A. R., Grass, L., Porter, A., Little, S., and Sotiropoulou, G. (2000) *Clin. Biochem.* **33,** 369–375
30. Diamandis, E. P., Yousef, G. M., Luo, L. Y., Magklara, A., and Obiezu, C. V. (2000) *Trends Endocrinol. Metab.* **11,** 54–60
31. Jancarik, J., and Kim, S.-H. (1991) *J. Appl. Crystallogr.* **24,** 409–411
32. Otwinowski, Z. (1993) in *Proceedings of the CCP4 Study Weekend: Data Collection and Processing* (Sawyer, L., Isaacs, N., and Bailey, S., eds) pp. 56–62, SERC Daresbury Laboratory, Warrington, UK
33. Otwinowski, Z., and Minor, W. (1997) *Methods Enzymol.* **276,** 307–326
34. Matthews, B. W. (1968) *J. Mol. Biol.* **33,** 491–497
35. Brunger, A. T., Adams, P. D., Clore, G. M., DeLano, W. L., Gros, P., Grosse-Kunstleve, R. W., Jiang, J. S., Kuszewski, J., Nilges, M., Pannu, N. S., Read, R. J., Rice, L. M., Simonson, T., and Warren, G. L. (1998) *Acta Crystallogr. Sec. D Biol. Crystallogr.* **54,** 905–921
36. Jones, T. A., Zou, J. Y., Cowan, S. W., and Kjeldgaard, M. (1991) *Acta Crystallogr. Sec. A* **47,** 110–119
37. Dayhuff, T. J., Gesteland, R. F., and Atkins, J. F. (1992) *BioTechniques* **13,** 500–503
38. Pearson, W. B. (1998) *J. Mol. Biol.* **276,** 71–84
39. Etzold, T., and Argos, P. (1993) *Comput. Appl. Biosci.* **9,** 49–57
40. Feng, D. F., and Doolittle, R. F. (1987) *J. Mol. Evol.* **25,** 351–360
41. Henikoff, S., and Henikoff, J. G. (1992) *Proc. Natl. Acad. Sci. U. S. A.* **89,** 10915–10919
42. Felsenstein, J. (2001) *PHYLIP*, version 3.5+, University of Washington, Seattle, WA
43. Strimmer, K., and von Haeseler, A. (1996) *Mol. Biol. Evol.* **13,** 964–969
44. Jones, D. T., Taylor, W. R., and Thornton, J. M. (1992) *Comput. Appl. Biosci.* **8,** 275–282
45. Schwartz, R. M., and Dayhoff, M. O. (1979) in *Atlas of Protein Sequences and Structure* (Dayhoff, M. O., ed) Vol. 5, pp. 353–358, National Biomedical Research Foundation, Washington, D. C.
46. Bock, C. W., Kaufman, A., and Glusker, J. P. (1994) *Inorg. Chem.* **33,** 419–427
47. Birktoft, J. J., Kraut, J., and Freer, S. T. (1976) *Biochemistry* **15,** 4481–4485
48. Scarisbrick, I. A., Towner, M. D., and Isackson, P. J. (1997) *J. Neurosci.* **17,** 8156–8168
49. Swofford, D. L. (2001) *PAUP**, version 4.0+, Sinaeur Associates, Sunderland, MA
50. Scarisbrick, I. A., Blaber, S. I., Lucchinetti, C. F., Genain, C. P., Blaber, M., and Rodriguez, M. (2002) *Brain* **125,** 1–14
51. Drinkwater, C. C., Evans, B. A., and Richards, R. I. (1987) *Biochemistry* **26,** 6750–6756
52. Blaber, M., Isackson, P. J., and Bradshaw, R. A. (1987) *Biochemistry* **26,** 6742–6749
53. Braun, P. J., Hofsteenge, J., Chang, J. Y., and Stone, S. R. (1988) *Thromb. Res.* **50,** 273–283
54. Blaber, M., Isackson, P. J., Burnier, J. P., Marsters, J. C. J., and Bradshaw, R. A. (1993) *Protein Sci.* **2,** 1210–1219
55. Hedstrom, L., Szilagyi, L., and Rutter, W. J. (1992) *Science* **255,** 1249–1253
56. Perona, J. J., and Craik, C. S. (1995) *Protein Sci.* **4,** 337–360

57. Huang, C., Li, L., Krillis, S. A., Chanasyk, K., Tang, Y., Li, Z., Hunt, J. E., and Stevens, R. L. (1999) *J. Biol. Chem.* **274,** 19670–19676
58. Varallyay, E., Pal, G., Patthy, A., Szilagyi, L., and Graf, L. (1998) *Biochem. Biophys. Res. Commun.* **243,** 56–60
59. Nakajima, N., Sugimoto, M., Ishihara, K., Nakamura, K., and Hamada, H. (1999) *Biosci. Biotechnol. Biochem.* **63,** 2031–2033
60. Oka, T., Hakoshima, T., Itakura, M., Yamamori, S., Takahashi, M., Hashimoto, Y., Shiosaka, S., and Kato, K. (2002) *J. Biol. Chem.* **277,** 14724–14730
61. Bode, W., Chen, Z., Bartels, K., Kutzbach, C., Schmidt-Kastner, G., and Bartunik, H. (1983) *J. Mol. Biol.* **164,** 237–282
62. Page, R. D. M. (1996) *Comput. Appl. Biosci.* **12,** 357–358
63. Hedstrom, L., Lin, T. Y., and Fast, W. (1996) *Biochemistry* **35,** 4515–4523